Mine Water and the Environment (2019) 38:136–147
https://doi.org/10.1007/s10230-018-0549-6

TECHNICAL ARTICLE

Fracture Characteristics of Overlying Bedrock and Clay Aquiclude Subjected to Shallow Coal Seam Mining

Zhiguo Liu[1,2] · Zhenli Fan[1,2] · Yujun Zhang[1,2]

Received: 9 December 2017 / Accepted: 5 June 2018 / Published online: 13 June 2018

Abstract

Some of the coal deposits in the northwest region of China are at relatively shallow depths, covered by a thin layer of bedrock and a thick layer of wind-blown sand. We studied the mechanics and permeability of a clay aquiclude by X-ray diffraction and triaxial loading tests and the fracturing of the overlying bedrock and aquiclude in physical simulation tests. The results indicate that if the bedrock thickness is 90 m or more, the height, distribution pattern, and damage to the water-conducting fractured and caving zones ("belts") are normal. If the bedrock thickness is 30 m or less, the "three belts make one" phenomenon occurs, and caving extends into the soil layer; the overlying rock is completely perforated by vertical fractures and the collapse spreads to the surface. When the bedrock thickness is between 30 and 90 m, the height of the water-conducting fractured zone is inhibited by the weathered rock and cohesive soil layers, and the height of the "two belts" is significantly decreased. This can be used to prevent and control coal mine water hazard.

Keywords Water hazard · Mining disturbance · Fracture evolution · Water-conducting fractured zone

Introduction

Estimates suggest that coal from the northwest region of China accounts for over 70% of the nation's coal production (Yuan et al. 2017, 2018; Zhang et al. 2017a, b). Among the various mines in this region, the Shenfu-Dongsheng coalfield has large coal reserves. The main mineable coal seam of this coalfield is characterized by shallow buried depth, thin bedrock, and thick wind-blown sand (Li et al. 2017; Wang et al. 2017). The main aquifers in the area are the water-rich, wind-blown sand layer and the Salawusu Formation aquifer. When the mining-associated collapse belt and water-conducting fractured zone reach the fourth series of the wind-blown sand layer and the Salawusu Formation aquifer, the accumulated water poses a serious threat to coal mine production, and causes heavy water resource depletion and environmental damage. However, the distribution of the soil layer provides an option to prevent and control water resource damage in this type of coal mine (Miao et al. 2008), because there are varying thicknesses of the fairly stable loess (Lishi Formation) and red soil (Baode Formation) beneath the Salawusu Formation aquifer and above the bedrock (Chen and Wang 2015; Gu 2016; Liu et al. 2017).

Several studies have been conducted on mining pressure and strata control of mining of shallow buried coal seams, the mechanism and techniques of water hazard control, and environmental management of the mining area, and significant breakthroughs have been achieved. Huang et al. (1999) and Huang (2005, 2009, 2010a) systematically summarized the basic rules and characteristics of mine pressure during shallow coal seam mining, elaborated the scientific definition of a shallow coal seam, proposed a temporary unstable "short masonry girder" of the key layer of the shallow coal seams and an unstable "step rock beam," studied the load transmission and the roof dynamic structural theory, obtained the distribution rule of the dynamic load on the key layer of the thick sand soil, and revealed the failure mechanism for the thick sand layer. Fan and Jiang (2003, 2004) and Fan (2005) performed studies on the hydrolytic

Electronic supplementary material The online version of this article (https://doi.org/10.1007/s10230-018-0549-6) contains supplementary material, which is available to authorized users.

✉ Zhenli Fan
fanzhenli@qq.com

[1] Coal Mining and Designing Branch, China Coal Research Institute, Beijing 100013, China

[2] Coal Ming and Designing Department, Tiandi Science & Technology Co., Ltd, Beijing 100013, China

and mechanical properties of the clay layer, and measured the related mechanical parameters. The authors pointed out that the water-resistant clay layer inhibited crack evolution. Based on geological exploration data, Li and Ye (2000) preliminarily obtained partial hydrolytic parameters of the water-resistant clay layer before and after coal mining by combining field engineering geological surveying and mapping, and in situ and laboratory tests. Ma et al. (2008) used 3-D numerical simulation software to simulate the initiation, development, and closure of the water-conducting fractures of the overburden, and revealed the related mechanism. Importantly, most studies were conducted by viewing the soil layer as the load action, and revealing its water-resistance. However, relatively little attention has been paid so far to the inhibitory effect of the soil layer on the height of the water-conducting fractured zone and the variation rules of the overburden rock failure. Zhang et al. (2014) quantified the primary factors influencing development of water-conducting zones within solid backfill mines based on the overburden movement and deformation characteristics. Liu et al. (2015) used numerical modeling to determine the height of water-conducting fractured zones during longwall mining of shallow coal seams. Also, various methods, such as electrical monitoring, have been used to identify water-conducting fractured zones (Su and Yue 2017, Su et al. 2016; Zhang and Liu 2012; Zhang et al. 2017a, b; Miao et al. 2011; Zhou et al. 2016). Christopher et al. (2017) assessed the potential impacts of longwall mining to surface and subsurface water bodies and Zhang et al. (2010, 2011) discussed the mechanism and basic requirements for aquifer protection during longwall mining. Karacan and Goodman (2009) reported hydraulic conductivity changes and influential factors in longwall overburden using slug tests in gob gas vent holes.

However, the effects of shallow coal seam mining on the physical properties and movement of water, the closing of fractures in the clay aquiclude, and the damage height of the composite structure of the overburden rock and clay aquiclude are different from those of traditional bedrock formations. Therefore, studying the nature of the clay aquiclude using rock samples is insufficient. It should also be analyzed from the perspective of "the entire layer", and incorporated into the process of the mining disturbance (Hu et al. 2018; Xia et al. 2017).

In this study, the mechanics and permeability of the clay aquiclude were first revealed via X-ray diffraction (XRD) analysis and triaxial loading tests. The fractures of the overlying bedrock and clay aquiclude were then observed in a physical simulation test. Subsequently, the influence of the thickness of the bedrock and red soil on the evolution of fractures in the overlying strata was elaborated. Finally, the fracture characteristics of the shallow bedrock and clay aquiclude were obtained.

Overview of the Study Area

The Yushenfu mining area of the Shendong coalfield consists of the Yushen and Shenfu mines, whose strata can be seen in the geologic column (Supplemental Fig. 1). The strata can be divided into five types: sand and soil-based, sand-based, soil-based, bedrock, and burnt rock (Li and Ye 2000). The sandy layer includes the Salawusu formation. The clay aquiclude mainly refers to the Lishi loess and hipparion red soil. The aquifer mainly includes the water-bearing sand-layer, the weathered bedrock aquifer, and the burnt rock aquifer. The sand-layer aquifer has moderate water yield. The Jurassic Zhongtong Yan'an formation is the coal-bearing stratum in this mining area and outcrops in many locations in the Shenfu mining area.

The Yushen mining area contains loess and red soil layers, which have some water resistance and protects the phreatic water of the overlying sand. This, along with the water-based clay, allows for safe coal mining, depending on the local conditions.

Mechanics and Permeability Property of the Clay Aquiclude

Mechanical Property of the Clay Aquiclude

The characteristic index of cohesive soil includes the initial molecular attraction of the soil particles as well as solidification formed by the cementation of the soil components. The magnitude of the internal friction angle and cohesion affect the shear strength of clay and determine its water-isolating and shear capacity. Therefore, the internal friction angle and cohesion are two mechanical indices of soil shear strength. Supplemental Fig. 2 shows the soil samples without any additional treatment (i.e. raw samples). Figure 1 shows the experimental device, sample preparation, and the soil sample after testing. Table 1 lists the basic physical and mechanical indices of the clay aquiclude. The test results show that the samples have obvious viscous soil characteristics.

The plasticity index is the difference between the liquid and plastic limits of the soil over its range of water content in the plastic state, and decreases as the water content increases. Because the plasticity index partly reflects the factors that affect the viscosity of the soil, the greater the plasticity index, the finer the soil particles, the larger the specific surface area, the higher the soil clay or hydrophilic mineral (such as montmorillonite) content, and the greater the change of water content of soil in a plastic state range.

The liquidity index determines the soil's physical state; the less the liquidity index, the harder the soil. According to the results of the experiment (Table 2), the plastic limit

of the Lishi loess is 20.1, its liquid limit is 25.1, its water content is 70%, and its plasticity index is 5. The soil is in a hard state, and is a sub-sand soil type. The liquid and plastic limits of the red soil are larger than those of the loess, and its plasticity index is 7.9, which indicates clay soil with moderate liquid limit. The liquid index is small, and the state of the soil is hard plastic, with high strength and low compressibility.

Expansion Property of Clay Aquiclude

Many factors can influence the expansion property of clay, such as clay content, organic matter content, clay mineral type, and composition of exchangeable cations, among which the clay content and mineral type play key roles. Mineral compositions in soil generally refers to kaolinite, illite, and montmorillonite, which have the characteristics of expansion, contraction, absorption, dispersion, condensation, adhesive, and plasticity. These are the main factors that control the soil's physical and mechanical properties and interaction with water, as well as an important basis for evaluating the water-resistance and mining-degeneration resistance of the unconsolidated formation. The results of the XRD analysis of the soil are shown in Tables 3 and 4.

Initially, the yellow soil layer is composed of loose, poorly cemented, and relatively uniform (in terms of size) particles; it is a silty soil but has a high sand content. XRD analysis shows that the soil contains quartz and feldspar minerals. The absolute content of quartz ranges between 45 and 50%, feldspar minerals comprise over 35%, and the absolute content of clay mineral is only about 10%. Based on the distribution of particles in the loess layer, the water storage space was found to be limited, with poor hydraulic conductivity. The clay minerals in this layer are mainly mixed layer illite–montmorillonite and illite. This suggests that its water stability is satisfactory and that its softening deformation characteristics are relatively weak because of the low clay content.

The core of the red soil layer in the Jingle group is deep red and well cemented. Gravel, with different diameters, can be found between the sticky components. XRD analysis show that the soil is mostly quartz (between 45 and 50%) and clay minerals (between 23.7 and 35.5%). Therefore, according to the mineral composition, the red soil of the Jingle group should be a claystone. Except for a small amount of grit, the particle gravel diameter was found to be small with good uniformity. It mostly consists of deep red viscous grains with good water resistance. Concerning the absolute clay mineral content, the main clays are illite–montmorillonite and illite, and these show obvious softening deformation characteristics under the influence of water. The test results indicated that the absolute clay mineral content of the red soil layer is high and determines its water stability. The water-resistance of the red soil layer is good and it expands somewhat when wet.

The expansibility of cohesive soil is mainly characterized by its linear expansion rate (expansion rate with side constraint), free expansion rate, and expansion force. The rate of linear expansion depends on the degree of clay compaction, natural moisture content, and soil structure. The free expansion rate is the expansion capacity without the influence of structural force, which illustrates the trend of the expansion. These two indices were chosen to evaluate the swelling property of the clay layer and a dilatometer was used to determine the linear expansion and free expansion rate of the loess and red soil samples (Table 5). It can be seen that there is some difference: the red soil's dilatability with side constraint is better due to its higher degree of compaction and greater mineral content. As the viscous soil expands, the fractures are blocked and its permeability decreases. Many tiny fractures are produced due to the mining and the shear pressure in the mine soil. If the expansion of the soil is better, cracks will develop during mining; however, they close on their own, reducing the height of the water-conducting fractured zone.

Seepage Property of Clay Aquiclude

The original permeability data of the red soil and loess were obtained from a water head regulation test. The test results showed that the permeability of the loess and red soil were $\approx$0.86–0.125 and $\approx$0.0179–0.0275 m/day, respectively.

Triaxial permeability measurement tests of the raw soils were conducted under different stress paths. After soil sample preparation, the entire stress–strain loading was performed on the original red soil using its original confining pressure. The permeability coefficient of the samples was measured before loading, and before, upon, and after reaching their ultimate strength. Figure 2a shows the experimental chamber. The failure characteristics of the raw soil after triaxial loading are displayed in Fig. 2b. It can be seen from these figures that the raw soil fails diagonally and appears to show obvious shear failure phenomenon.

The variation in permeability coefficient (test results) of the raw soil during triaxial loading is shown in Fig. 3. Based on these results, the following conclusions are made: (1) the stress–strain curves of the raw soil show plastic, yield, and residual deformation. (2) The permeability coefficient of cohesive soil declines significantly during the initial triaxial loading of the raw soil and minimally when entering the yield stage, but it declines even more after reaching maximum intensity. (3) After destruction of the raw soil, the permeability coefficient does not increase with the occurrence of the shear fracture, but continues to decline.

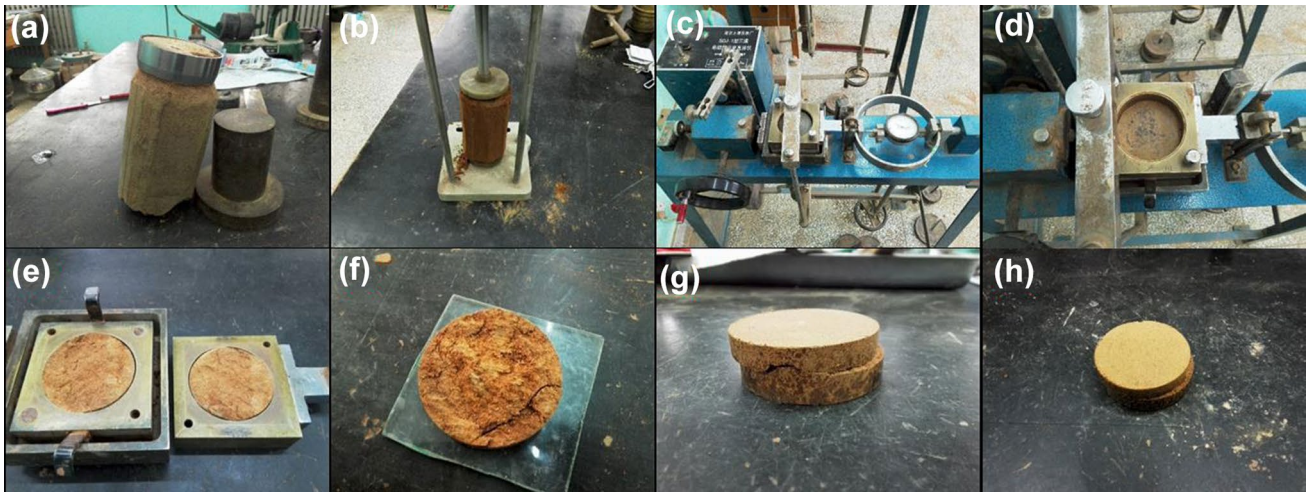

Fig. 1 Experimental device, sample preparation, and the soil sample after test. **a** Original ring knife sample preparation. **b** Original triaxial sample preparation. **c** Electric direct shear meter. **d** Electric direct shear meter after sample loading. **e** Direct shear test of raw soil sample under 100 kPa pressure. **f** Direct shear test of raw soil sample under 200 kPa pressure. **g** Direct shear test of briquette soil sample under 100 kPa pressure. **h** Direct shear test of briquette soil sample under 200 kPa pressure

Table 1 Test results of mechanical parameters of cohesive soil

Lithology	Moisture content/%	Density/(g/cm^3)	Internal friction angle/°	Compressive strength/kPa
Loess	9.59	1.92	38	189
Red soil	21	2.18	37	192

Table 2 Test results of indices of basic water-physical properties of clay aquiclude

Lithology	Liquid limit/%	Plastic limit/%	Plasticity index	Liquidity index	Saturability/%
Loess	25.1	20.1	5	−2.27	70
Red soil	35.4	27.5	7.9	0.22	75.6

Fracture Evolution in the Shallow Bedrock and Clay Aquiclude

Overview of Test Prototype Geology

According to the aforementioned analysis, the main formation structure of the Yushen mining area is sand- and soil-based. In this type, the sand is a shallow aquifer, the soil is a loess, and a red soil layer is widely deposited beneath the submerged aquifer. The base is the rock-weathering zone and the original bedrock. The thickness of the coal seam is ≈1.44–8.80 m, with an average value of 7.5 m. The buried depth of the coal seam is ≈130–170 m. The original strata conditions are presented in Supplemental Table 1.

Table 3 Results of minerals X-ray diffraction analysis

No.	Mineral types and content (%)					Total clay minerals content/%
	Quartz	Potash feldspar	Soda feldspar	Calcite	Hornblende	
Loess1	48.5	14.0	24.1	–	2.9	10.5
Loess 2	45.2	13.2	30.2	–	0.6	10.8
Red soil 1	48.9	5.6	10.0	–	–	35.5
Red soil 2	45.3	3.5	10.4	17.1	–	23.7

Table 4 Results of X-ray diffraction of clay minerals

No.	Relative content of clay minerals/%						Ratio of mixed-layer S/%	
	S	I/S	I	K	C	C/S	I/S	C/S
Loess 1	–	25	44	9	22	–	70	–
Loess 2	–	33	43	8	16	–	60	–
Red soil 1	–	60	23	8	9	–	75	–
Red soil 2	–	44	32	13	11	–	70	–

S smectite, *I/S* illite mixed layer, *I* glimmerton, *K* kaolinite, *C* chlorite, *C/S* green slip layer

Table 5 Expansion parameters of viscous soil

Lithology	Free swelling ratio/%	Expansion rate with side constraint under no pressure/%	Expansion rate with side constraint under 50 kPa pressure/%
Loess	43.6	25.2	8.6
Red soil	50	29.7	10

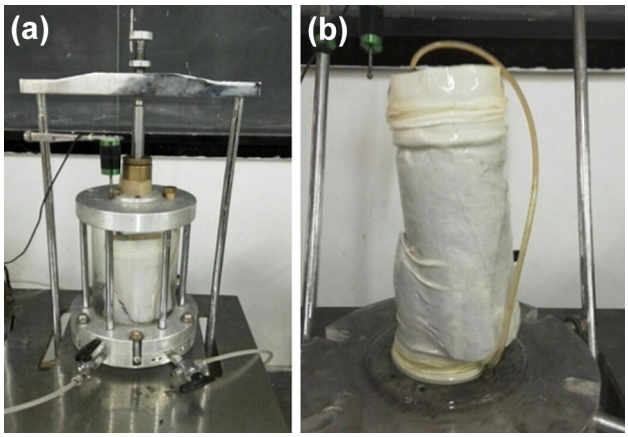

Fig. 2 Experimental chamber and failure characteristics of raw soil and briquette soil after triaxial loading. **a** Experimental chamber. **b** Failure characteristics of raw soil after triaxial loading

Experimental Design of a Similar Simulation Test

Physical simulation experiments of mining have mainly focused on the working face roof and the rock surrounding the roadway; moreover, in most cases, brittle materials were used. The aim of this experiment was to understand the similarity between deformation and destruction of the aquifer by considering the plasticity of the aquifer. Special research on materials similar to the clay aquiclude with strong plasticity have been conducted in recent years. For example, Huang (2000) developed a fluid–solid coupling experimental device, and investigated the simulation of clay aquiclude using paraffin wax as coagulating agent and sand as aggregate. Huang and Liu (2006) preliminarily simulated the influence of the collapse of bedrock on the destruction of the aquifer using paraffin wax as a cementing agent, but they found the stability of the paraffin wax to be poor; it was more brittle when cool and more plastic when warm. Thus, paraffin wax is not an ideal coagulant. Huang et al. (2010b) found that silicone oil is a better, low-intensity, non-hydrophilic cementing agent, and that vaseline is a better cementing material for plastic deformation. Based on these findings, a similar simulation material with better strength and hydrolytic properties was developed. However, similar conditions for plastic deformation are not available.

1. Selection of similar materials

According to the similarity principle, the material used in the model experiment must have similar physical and mechanical properties with the prototype material (Zou and Lin 2018). The base rock and weathering layer can be made of sand, gypsum, and calcium carbonate, clean river sand was selected as the aggregate, and gypsum and large white powder was used as cementing materials. For the coal, river sand and coal ash were used as an aggregate, and gypsum and large white powder were used as materials that were similar to the cementing material. River sand, clay, water, and oil were selected as materials representing the soil layer. The river sand was used as aggregate to provide strength, clay was used as a cementing agent to improve material plasticity, and oil and water were used to adjust the strength and plasticity of the materials. The red soil was simulated with a sand-to-soil ratio of 1:1 and an oil-to-soil ratio of 1:5; the loess was simulated with a sand-to-soil ratio of 1:1 and oil-to-soil ratio of 1:4. The physical model of the similar simulation test is shown in Supplemental Fig. 3. The mechanical parameters of the loess and red soil are listed in Supplemental Table 2.

2. Determination of similar conditions

Parameters that should be similar include geometric proportion l, unit weight γ, time t, rock strength R, elastic modulus E, internal friction angle φ, and Poisson's ratio μ. Previous simulations mainly considered similarity in strength.

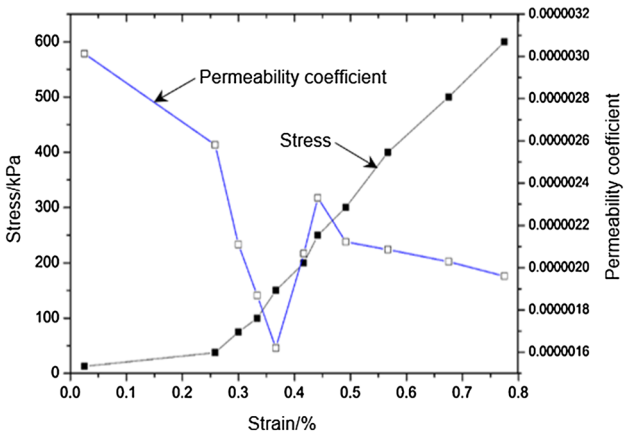

Fig. 3 Stress–strain curves and variation in permeability coefficient of raw soil

This test also accounted for the similarity of deformation parameters, specifically:

Geometric similarity ratio: $\alpha_l = \frac{l_p}{l_m} = 200$; unit weight similarity ratio: $\alpha_\gamma = \frac{\gamma_p}{\gamma_m} = 1$;
Time similarity ratio: $\alpha_t = \frac{t_p}{t_m} = 14.14$; Displacement similarity ratio: $\alpha_s = \alpha_l = 200$;
Strength, elastic modulus and adhesion force similarity ratio: $\alpha_R = \alpha_E = \alpha_C = 200$;
Internal friction angle and Poisson's ratio similarity ratio: $\alpha_\varphi = \alpha_\mu = 1$.

Because the soil layer was mainly used to simulate plastic deformation of the soil layer under additional stress, the ratio of similarity of plasticity stress of the soil layer was determined, namely $\alpha_{Ep} = \alpha_\sigma = 200$. The other parameters were the same as those for the bedrock.

Analysis of the Experimental Results

The immediate roof of the coal seam collapsed when the working face of the model was pushed 5 cm from the open-off cut (Fig. 4a–c). When it was pushed to 10 cm, the immediate roof collapsed again. When the distance was 20 cm, the first weight occurred, and the first weighting interval was 40 m. As the working surface continued to advance (Fig. 4d), the water-conducting fractured zone entered the weathering zone to achieve bed separation for the first time. As the working face gradually advanced to 150 cm, the interface between the soil and bedrock presented bed separation and bending deformation, and some small cracks occurred in the weathering zone. However, they compacted quickly as the working face advanced. As the working surface continued to advance, the bed separation in the soil layer developed continuously upward, and the water-conducting fractured zone entered the lower part of the soil layer, and formed a step slip surface on the edge. Thus, it can be seen that the cohesive soil layer in this area, influenced by rock caving, gradually produced local bed separation and bending subsidence from bottom to top, parallel to the bedding plane. The fracture belt no longer developed upward. As the compaction of the space of the lower part of bed separation continued, bed separations developed upward, and the soil layer basically remained in the bending subsidence zone (Fig. 4e–f).

As the working surface continued to advance rapidly, the cohesive soil layer and water-bearing sand layer of the curved zone subsided along with the bedrock. Tension cracks formed in the surface tension zone on both sides of the goaf. Results of the model bed separation and the height of the water-conducting fractured zone and subsidence show that, due to the thick bedrock, the bedrock will be fractured, bend, produce bed separation, and eventually rupture as the coal seam is mined; however, the water-protecting soil layer remains stable, and gradually forms a subsidence basin. Meanwhile, the bedrock weathering zone and soil layer inhibit the growth of a water-conducting fractured zone (Fig. 4g, h). Besides, the edge of the surface subsidence basin presents a more obvious sinking step due to the shallow buried depth and thin bedrock (Fig. 4g).

Effect of Bedrock Thickness and Red Soil Thickness on the Evolution of Fractures in the Overlying Strata

Numerical Model Establishment and Numerical Scheme

Since the water-resistant layer is mainly composed of a clay layer with apparent plasticity, the prototype was based on the formation structure of the "sand layer–loess layer–red soil layer–bedrock weathering belt–bedrock" in the Yushen mining area. The structure of the numerical model is shown in Supplemental Fig. 4.

The specific provisions are: (1) the left and right boundaries of the model constrain the horizontal displacement, so the velocity vector and displacement vector of the horizontal direction are zero. (2) The lower boundary of the model is fixed in both horizontal and vertical directions, that is, the lower boundary of the model is the full constraint boundary. (3) The upper boundary of the model is a free boundary.

The Mohr–Coulomb plastic model was adopted for the numerical model, which considers the physical and mechanical parameters of the rock and the structural plane of the surrounding rock (Supplemental Tables 3 and 4). The

simulation scheme was determined in accordance with the research. By keeping the thickness of the 4th system loose bed and loess layer constant, we changed the thickness of the bedrock and red soil layer to simulate the influence of different thickness of bedrock and soil layer on the overlying rock (soil) migration rule.

Effect of Bedrock Thickness on the Characteristics of the Fractures of the Overlying Strata

Figure 5 shows the fractures of the overlying strata and their distribution with different bedrock thickness (i.e. 30, 50, 70, and 90 m) during working face advancement when the mining height is 7 m and the red soil layer is 30 m thick.

As can be seen from Fig. 5, the buried depth is relatively small, and the marginal surface of the goaf shows obvious step-shaped subsidence when the bedrock is 30 m thick. The bedrock layer breaks from the middle and both ends of the coal wall, and the fractures extend to the surface. Nearly vertical fractures appear behind the coal wall and cut the working face, eventually expanding and extending to the upper sand bed. As shown in Fig. 5a, the compaction effect of the middle-roof-fall rock stratum is good. At this time, no "three belt" exists, and the destructive pattern of the overlying rock (soil) is downward.

Subsidence of the surface significantly decreases with an increase in bedrock thickness, indicating that the thicker the bedrock, the stronger the suppression to surface subsidence. The upper bedrock layer fractures and forms a hinged structure to bear the upper bedrock and the loose layer. The surface slowly sinks down without steps, and the overlying strata forms a collapse belt and a fractured belt (two belts) in the vertical direction. The bedrock fully collapses, and the collapse belt is fully developed, but the height, distribution pattern, and the

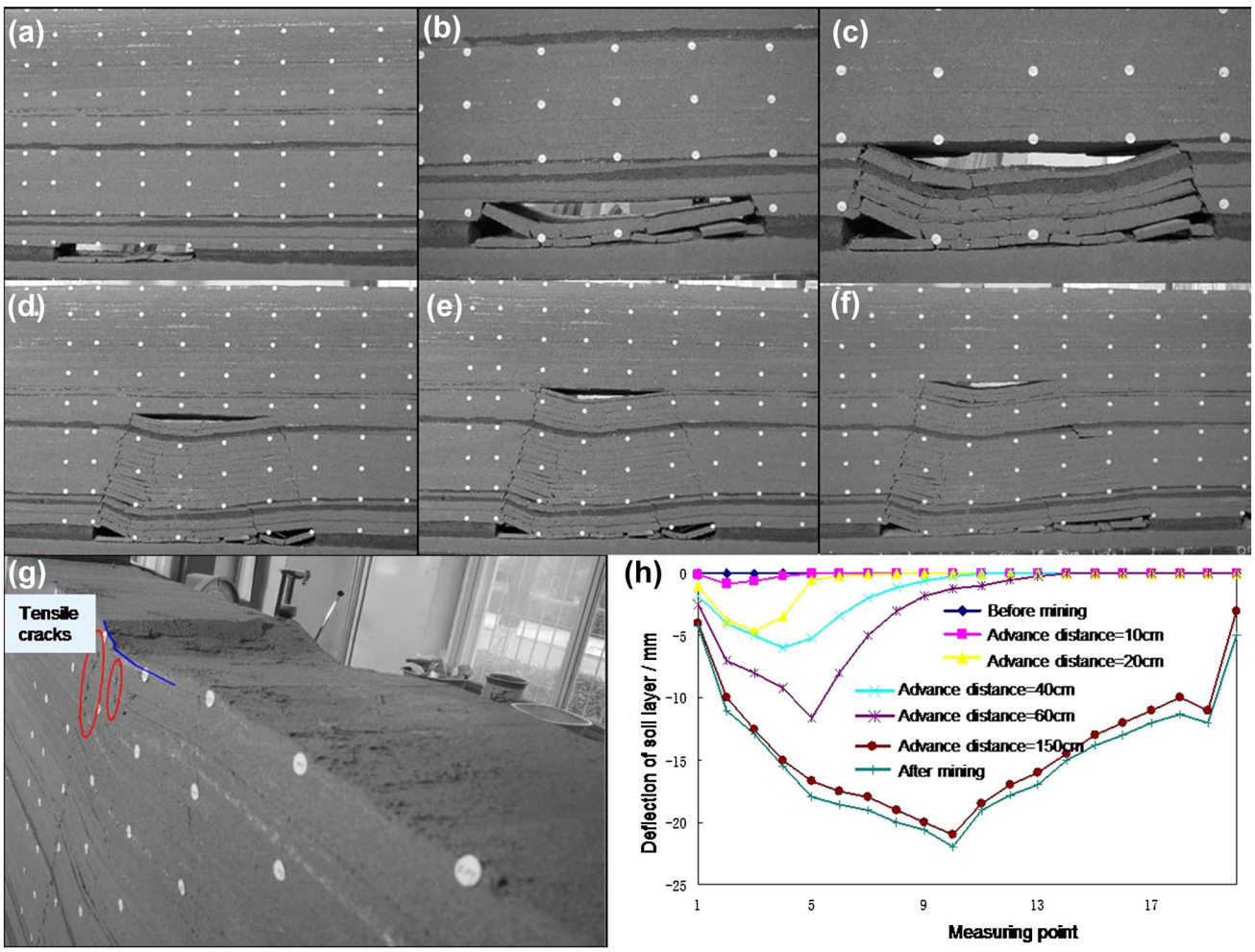

Fig. 4 Results of the similar simulation test. **a** Immediate roof collapses. **b** The second collapse of the immediate roof. **c** The first weight of the upper roof. **d** Water-conducting cracks enter the weathering zone. **e** Bed separation between the soil layer and the bedrock boundary. **f** Bed separation in the soil layer. **g** Surface collapse. **h** Curves of deflection of the soil layer

degree of damage of the water-conducting fractured zone are not fully developed due to the soil layer effect. When the thickness of the bedrock is 50 m, the fractured belt enters the lower part of the soil layer, and the height of the fractured belt is about 56 m (Fig. 5b). When the thickness of bedrock is 70 m, the fractured belt does not develop after entering the interface of the soil layer and the bedrock, and the height of the fractured belt is 70 m (Fig. 5c). Finally, when the bedrock is 90 m thick, the height of the water-conducting fractured zone is about 85 m after mining is complete because of the increased bedrock thickness and the minor influence of the soil layer on the height of the water-conducting fractured zone (Fig. 5d). Thus, the developed height increases.

The simulation results show that for shallow depth conditions, the development height of the "two belts" increases gradually with an increased bedrock thickness. If the bedrock is thin enough, the effect of mining shows holistic subsidence, and there are no bed separation fractures between the rock and soil layers. Moreover, the development of "two belts," especially the development of caving zone height, distribution pattern, and extent of damage, is normal, because the simulation study area is hard rock strata. However, the height of the water-conducting fractured zone obviously decreases due to the inhibitory effect of the soil layer on the height and extent of damage of the water-conducting fractured zone, and the development is not complete. Even if the fractures at the top enter the soil layer, they will close as the working face rapidly advances.

Effect of Red Soil Thickness on the Fracture Characteristics of the Overlying Strata

Figure 6 shows the characteristics of the fractures of the overlying strata and their distribution for different red soil layer thicknesses (i.e. 10, 20, and 30 m) while the working face advances when the mining height is 7 m. The simulation results show that the height, distribution pattern, and damage extent of the caving zone are normal when the bedrock is 50 m thick. However, the height and extent of damage to the water-conducting fractured zone are inhibited by the soil layer, so the height of the water-conducting fractured zone decreases and the fractured belt enters the lower part of the red soil layer.

A comparison of the results of the three schemes indicates that if the bedrock thickness remains the same and the soil layer has different heights, the thickness of the water-conducting fractured zone doesn't markedly change. As the soil layer thickens, the integral falling of the overlying rock in the overburden gob area is more obvious, and a high caving angle fractured group forms behind the coal wall and at the open-off cut at the working face. The compaction effect in the middle of the caving rock strata is better. Although the buried depth of the coal seam is shallow, due to the strong bearing-action and camber of the clay layer, it can combine

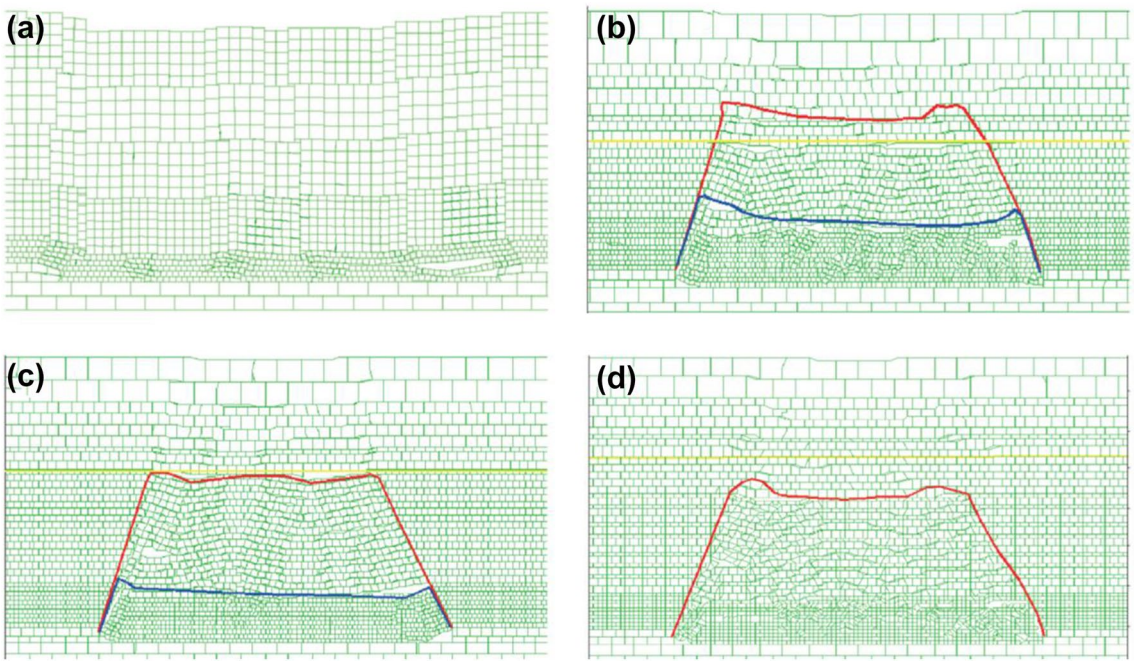

Fig. 5 Fissures characteristics of the overlying strata and their distribution under different bedrock thickness. **a** The bedrock thickness is 30 m. **b** The bedrock thickness is 50 m. **c** The bedrock thickness is 70 m. **d** The bedrock thickness is 90 m

with the thin bedrock to form a stable structure. At the same time, because the bedrock is thicker than the soil layer, it can form a stable bearing structure when the basic roof breaks, and so sliding instability does not occur. The strata continuously bends instead of fracturing.

Fracture Characteristics of the Bedrock and Clay Aquiclude

From the aforementioned analysis, it can be seen that due to the shallow burial depth, thin bedrock, and clay layer, the zoning features and the effects on the overlying rock/sand/soil will be different for the Yushen area than it would be if the seam being mined was deeper. The characteristics of the fracture development in the bedrock and clay aquiclude can be summarized as:

1. If the bedrock is 90 m thick, then "two belts" develop. The height, distribution pattern, and damage of the water-conducting fractured zone and caving zone are normal. However, due to the shallow mining depth, the height of the water-conducting fractured zone will decrease as the mining depth decreases.
2. If the bedrock is only 30 m thick, the "three belts make one" phenomenon occurs, and the caving extends into the soil layer. The overlying rock is completely perforated by vertical fractures and the collapse extends to the surface (Fig. 7).
3. When the bedrock thickness is greater than 30 m and less than 90 m, the height of the water-conducting fractured zone will be inhibited by the weathered rock and cohesive soil layers, and the height of the "two belts" will significantly decrease. As shown in Fig. 8a, if the cohesive soil is poorly consolidated, the development of the water-conducting fractured zone is suppressed, and the fractures will not develop into the cohesive soil layer. As shown in Fig. 8b, if the cohesive soil is well consolidated, the water-conducting fractured zone may enter the cohesive soil layer. However, even if it enters the clay layer, the water-conducting fractures will only exist for a short time, and the "two belts" will control the bedrock and cohesive soil layer.

Guiding Significance for Prevention and Control of Water Hazards

Water-conducting channels due to mining disturbance are key factors that influence the occurrence of water hazards. Therefore, decreasing damage of the overlying strata, especially for shallow coal seams with thin bedrock, is an important way to reduce or prevent this hazard. Our analysis indicates that the soil layer can significantly reduce the length of the water-conducting fractured zone, but that an atypical damage pattern forms due to the shallow depth. Based on the geological and mining conditions of the Yushen mining area, the following techniques can be used.

1. Reasonable selection of the mining method. Because the main coal seam of the Yushen mining area is thick, mechanized, longwall mining would normally be preferred. However, this approach would cause strong mining disturbance. Instead, slicing and filling mining methods should be used to reduce the mining disturbance.
2. Effective support of the working face. Movement of the overlying strata for a shallow burial depth depend on the fracture characteristics of the key strata. The support force of the working face determines, to some extent, the stability of the damage of the key strata. Therefore, effective support of the working face can control damage to the roof, which effectively reduces the length of the water-conducting fractured zone.
3. Rapid advance of the working face. The advancement velocity significantly affects the movement of the overlying strata and fracture development. The faster the working face advances, the slower the overlying strata sinks, and the less water-conducting fractures develop. Besides, rapid advance of the working face can quickly close the fractures, which, to some extent, restrains formation of the water-conducting channels.

Conclusions

In this study, first, the mechanics and permeability property of clay aquiclude were revealed via XRD analysis and triaxial loading tests, which provided fundamental parameters for the design of a similar simulation test and numerical simulation. The formation of fractures in the overlying rock (soil) was observed in the simulation test. Subsequently, the influence of bedrock and red soil thickness on the evolution of fractures in the overlying strata was elaborated. Finally, the fracture characteristics of shallow buried rock (soil) subjected to mining disturbance were obtained. The main conclusions are:

The soil layers in the Yushen mining area are cohesive, with good water-resistance and fracture resistance. This kind of soil compacts easily, and produces fractures that close easily, which can effectively inhibit the development of water-conducting fractures.

Due to the existence of the weathering zone and cohesive soil layer, bed separation first occurs after the water-conducting fractured zone enters the weathering zone. As the working face gradually advances to 150 m, the interface between the soil and bedrock shows bed separation and bending deformation, and some small cracks are produced in the weathering zone. However, these compact quickly as

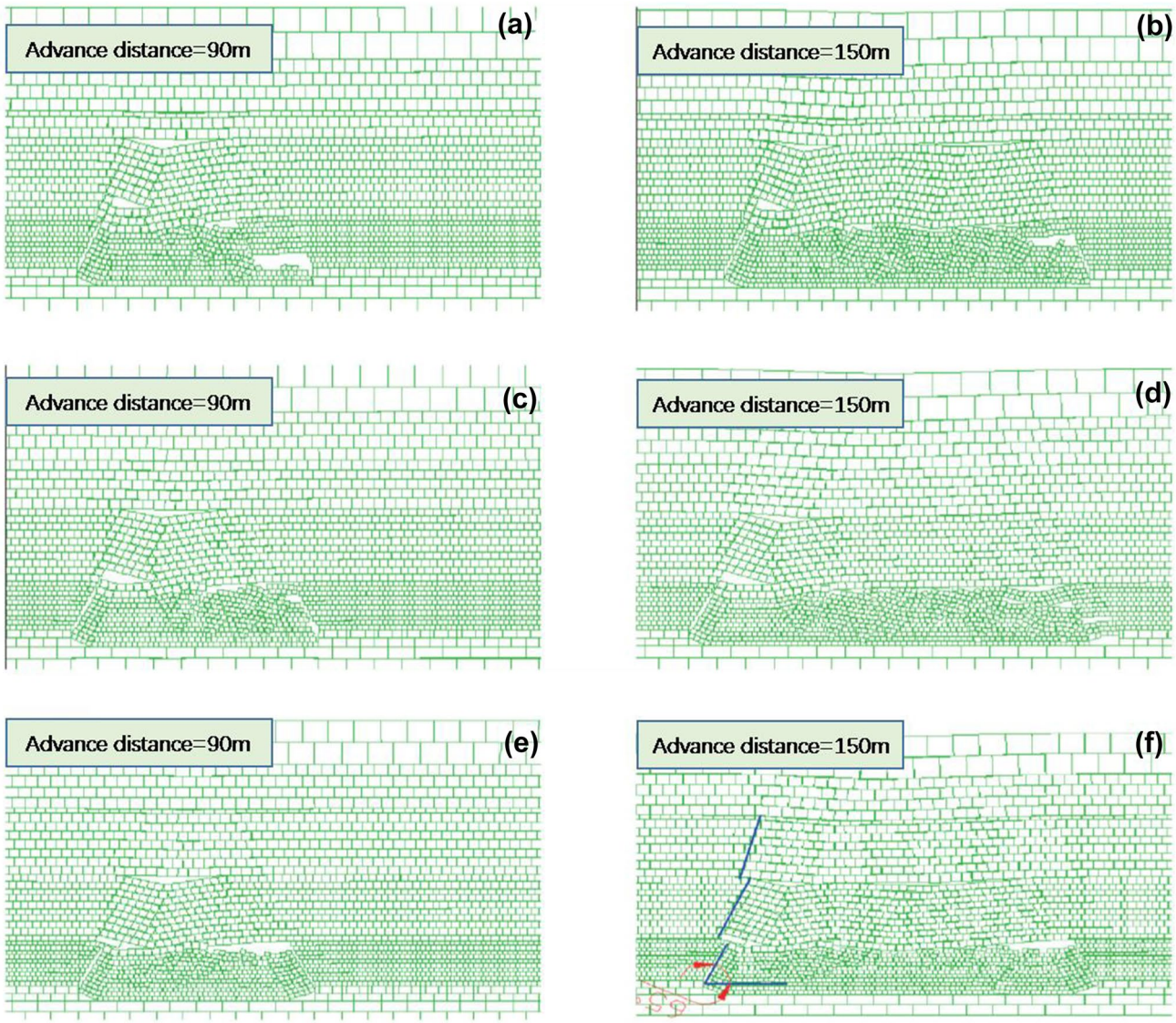

Fig. 6 The fissures' characteristics of the overlying strata and their distribution under different red soil layer thickness. **a** The red soil layer thickness is 10 m and the advance distance is 90 m. **b** The red soil layer thickness is 10 m and the advance distance is 150 m. **c** The red soil layer thickness is 20 m and the advance distance is 90 m. **d** The red soil layer thickness is 20 m and the advance distance is 150 m. **e** The red soil layer thickness is 30 m and the advance distance is 90 m. **f** The red soil layer thickness is 30 m and the advance distance is 150 m

the working face advances. As the working surface continues to advance, the bed separation in the soil layer continues to develop upward, and the water-conducting fractured zone enters the lower part of the soil layer, where it forms a step slip surface on the edge. As the mining face continues to rapidly advance, the cohesive soil and water-bearing sand layers of the curved zone subside along with the bedrock.

When the bedrock is at least 90 m thick, the "two belts" are fully developed, and the height, distribution pattern, and damage to the water-conducting fractured and caving zones are normal. However, due to the shallow mining depth, the height of the water-conducting fractured zone will decrease along with the mining depth. If the bedrock thickness is 30 m or less, the "three belts make one" phenomenon occurs, and the caving belt extends directly into the soil layer. The overlying rock is completely perforated by the vertical fractures and the collapse occurring outspread the surface. When the bedrock thickness is between 30 and 90 m, the height of the water-conducting fractured zone will be inhibited by the weathered rock and cohesive soil layers, and the height of the "two belts" will significantly decrease.

Decreasing the damage to the overlying strata is the key measure to prevent water hazard, especially for shallow coal seams with thin bedrock. The following techniques can be

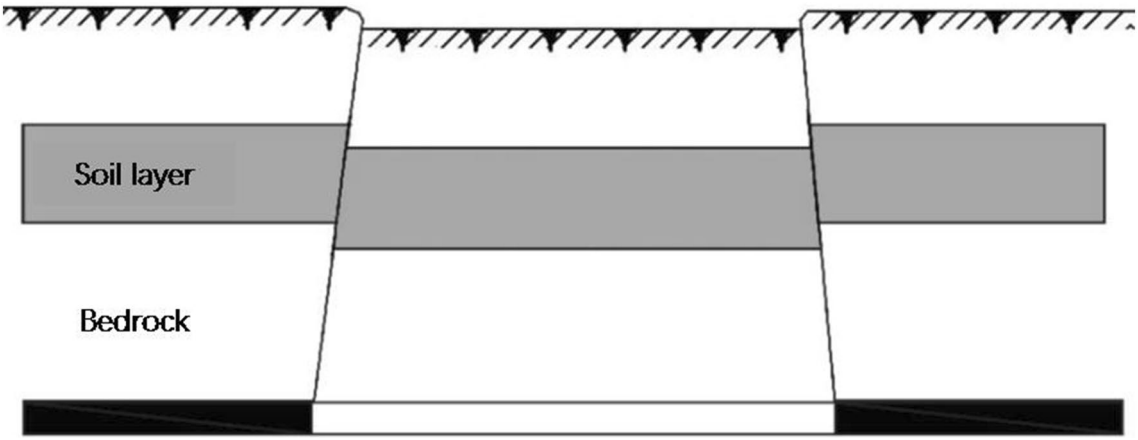

Fig. 7 Fissure characteristics of the shallow buried rock (soil) when the bedrock thickness is small enough, and the mining height is relatively large

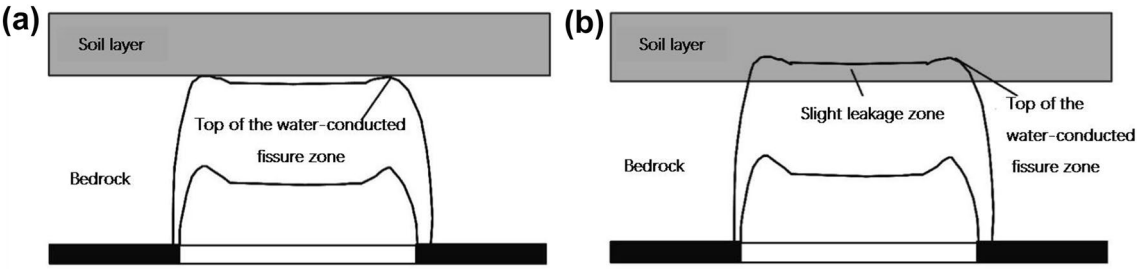

Fig. 8 Fissure characteristics of the shallow buried rock (soil) when the bedrock thickness is small. **a** The fissures extend to the bottom of the soil layer. **b** The fissures extend to the soil layer

used for this purpose: reasonable selection of the mining method, effective support of the working face, and rapid advance of the working face.

Acknowledgements This work was financially supported by the National Science and Technology Major Project of China (Grants 2016ZX05043005 and 2016ZX05045007) and National Natural Science Foundation of China (Grant 5170041013), which are gratefully acknowledged. We also thank the anonymous reviewers for their comments and suggestions to improve the manuscript.

References

Chen K, Wang X (2015) Analysis of the factors causing roof water inrush in coal seam mining with thin bedrock. Chem Eng Trans 46:679–684

Christopher N, Zacharias A, Gabriel B (2017) Assessment of potential impacts to surface and subsurface water bodies due to longwall mining. Int J Min Sci Technol 27:57–64

Fan L (2005) Discussing on coal mining under water-containing condition. Coal Geol Explor 33:50–53 (**in Chinese**)

Fan L, Jiang Z (2003) Research on coal mining under competent loose aquifer and properties of aquiclude in Yushen mining area. Coal Geol China 15:52–53 (**in Chinese**)

Fan L, Jiang Z (2004) Engineering geologic background of coal mining under water-containing condition in Yushen coal mining area. Coal Geol Explor 32:32–35 (**in Chinese**)

Gu D (2016) Technology development and engineering practice for protection and utilization of water resources in coal mining in Western China. Front Eng Manag. https://doi.org/10.15302/J-FEM-2016010

Hu Q, Tian C, Tan Y, Sun H, Dai L, Cao J (2018) Study of the hard roof mechanical properties in the process of repeated coal mining. J Chin Univ Min Technol 47:68–73 (**in Chinese**)

Huang Q (2000) Study on roof structure and rock strata control of shallow coal seam in longwall mining. China Univ of Mining and Technology Press, Beijing (**in Chinese**)

Huang Q (2005) Studies on load-transmitting factor of thick sandy soil layer on key roof stratum in shallow seam mining. Chin J Geotech Eng 27:672–676 (**in Chinese**)

Huang Q (2009) Simulation of clay aquifuge stability of water conservation mining in shallow-buried coal seam. Chin J Rock Mech Eng 28:988–992 (**in Chinese**)

Huang Q, Liu T (2006) Simulating test on the subsidence law of subsurface water resisting layer upon shallow coalbed mining. Coal Geol Explor 34:34–37 (**in Chinese**)

Huang Q, Qian M, Shi P (1999) Structural analysis of main roof stability during periodic weighting in longwall face. J Chin Coal Soc 24:581–585 (**in Chinese**)

Huang Q, Wei B, Zhang W (2010a) Study of downward crack closing of clay aquiclude in shallow-buried coal seam. J Min Saf Eng 27:35–39 (**in Chinese**)

Huang Q, Zhang W, Hou Z (2010b) Study of simulation materials of aquifuge for solid–liquid coupling. Chin J Rock Mech Eng 29:2813–2818 (**in Chinese**)

Karacan CO, Goodman G (2009) Hydraulic conductivity changes and influencing factors in longwall overburden determined by slug tests in gob gas ventholes. Int J Rock Mech Min Sci 46:1162–1174

Li W, Ye G (2000) Study on the engineering geological conditions of protected water resources during coal mining action in Yu-Shen-Fu Mine area in the North Shanxi Province. J Chin Coal Soc 25:449–454 (**in Chinese**)

Li S, Fan C, Luo M, Yang Z, Lan T, Zhang H (2017) Structure and deformation measurements of shallow overburden during top coal caving longwall mining. Int J Min Sci Technol 27:1081–1085

Liu X, Tan Y, Ning J, Tian C, Wang J (2015) The height of water-conducting fractured zones in longwall mining of shallow coal seams. Geotech Geol Eng 33:693–700

Liu J, Sui W, Zhao Q (2017) Environmentally sustainable mining: a case study of intermittent cut-and-fill mining under sand aquiclude. Environ Earth Sci 562

Ma L, Zhang D, Qiao J (2008) Physical simulation of water crack distribution characteristics in overlying strata under coal mining conditions. J Liaoning Tech Univ (Nat Sci) 27:649–652 (**in Chinese**)

Miao X, Pu H, Bai H (2008) Principle of water-resisting key strata and its application in water-preserved mining. J Chin Univ Min Technol 37:1–4 (**in Chinese**)

Miao X, Cui X, Wang J, Xu J (2011) The height of fissured water-conducting zone in undermined rock strata. Eng Geol 120:32–39

Su B, Yue J (2017) Research of the electrical anisotropic characteristics of water-conducting fissured zones in coal seams. Appl Geophys 14:216–224

Su B, Malekian R, Yu J, Feng X, Liu Z (2016) Electrical anisotropic response of water conducted fissured zone in the mining goaf. IEEE Access 4:6216–6224

Wang F, Duan C, Tu S, Liang N, Bai Q (2017) Hydraulic support crushed mechanism for the shallow seam mining face under the roadway pillars of room mining goaf. Int J Min Sci Technol 27:860–863

Xia B, Jia J, Yu B, Zhang X, Li X (2017) Coupling effects of coal pillars of thick coal seams in large-space stopes and hard stratum on mine pressure. Int J Min Sci Technol 27:965–972

Yuan L, Zhang T, Zhao Y, Ren B, Hao X, Xu C (2017) Precise coordinated mining of coal and associated resources: a case of environmental coordinated mining of coal and associated rare metal in Ordos basin. J Chin Univ Min Technol 46:449–459 (**in Chinese**)

Yuan L, Zhang N, Kan J, Wang Y (2018) The concept, model and reserve forecast of green coal resources in China. J Chin Univ Min Technol 47:1–8 (**in Chinese**)

Zhang S, Liu Y (2012) A simple and efficient way to detect the mining induced water-conducting fracturedd zone in overlying strata. Energy Proc 16:70–75

Zhang D, Fan G, Liu Y, Ma L (2010) Field trials of aquifer protection in longwall mining of shallow coal seams in China. Int J Rock Mech Min Sci 47:908–914

Zhang D, Fan G, Ma L, Wang X (2011) Aquifer protection during longwall mining of shallow coal seams: a case study in the Shendong coalfield of China. Int J Coal Geol 86:190–196

Zhang J, Jiang H, Deng X, Ju F (2014) Prediction of the height of the water-conducting zone above the mined panel in solid backfill mining. Mine Water Environ 33:317–326

Zhang J, Zhang Q, Spearing A, Miao X, Guo S, Sun Q (2017a) Green coal mining technique integrating mining-dressing-gas draining-backfilling-mining. Int J Min Sci Technol 27:17–27

Zhang S, Tang S, Zhang D, Fan G, Wang Z (2017b) Determination of the height of the water-conducting fracturedd zone in difficult geological structures: a case study in Zhao Gu No. 1 coal seam. Sustainability 9:1077. https://doi.org/10.3390/su9071077

Zhou D, Wu K, Li L, Yu J (2016) Impact of thick alluvial soil on a fractured water-conducting zone: an example from Huainan coal mine, China. J S Afr Inst Min Metall 431:440. https://doi.org/10.17159/2411-9717/2016/v116n5a9

Zou Q, Lin B (2018) Fluid–solid coupling characteristics of gas-bearing coal subject to hydraulic slotting: an experimental investigation. Energy Fuel 32:1047–1060